

Phase Coherence of Ultrafast Carriers in $\text{Bi}_2\text{Sr}_2\text{CaCu}_2\text{O}_{8+\delta}$ Thin Film

H. Murakami*, T. Kiwa*, N. Kida*, and M. Tonouchi*⁺
*Research Center for Superconductor Photonic,
 Osaka University*, and CREST-JST⁺,
 Suita, Osaka 565-0871, Japan*

T. Uchiyama, and I. Iguchi
*Department of Physics, Tokyo Institute of Technology, and CREST-JST,
 2-12-1 Ookayama, Meguro-ku, Tokyo 152-8551, Japan*

Z. Wang
Kansai Advanced Research Center, Communication Research Laboratory, Kobe 651-2492, Japan
 (Dated: December 2, 2024)

Time-domain terahertz-transmission spectroscopy was carried out on a c-axis oriented $\text{Bi}_2\text{Sr}_2\text{CaCu}_2\text{O}_{8+\delta}$ thin film. We directly extracted the complex conductivity and surface impedance at frequencies from 0.3 to 1.5 THz by numerically solving the observed complex transmittance without Kramers-Kronig analysis. The frequency-resolved imaginary part of the conductivity, σ_2 , showed measurable increase below the characteristic temperature (T^*) of about 210 K in $1.0 \text{ THz} < f$, and a rapid increase below the superconducting transition temperature (T_C) in $f < 0.5 \text{ THz}$. Correspondingly, frequency dependence of the density of supercarrier N_S showed a local maximum around $f \simeq 1.3 \text{ THz}$ below T^* and a rapid increase in $f < 0.5 \text{ THz}$ below T_C .

These results show that partial and short-range phase coherence takes place below T^* with an ultrafast correlation time of 1 ps or less, and also that the origin of the correlation is different from that of the long-range one below T_C .

PACS numbers: 74.25.-q, 74.25.Nf, 74.72.Hs

Normal state anomalies in underdoped high- T_C superconductors (HTSC) have been experimentally studied using many approaches, including NMR, neutron scattering, infrared conductivity, transport property, tunneling spectroscopy, and angle resolved photoemission spectroscopy. [1, 2, 3, 4, 5, 6] The main focus has been the possibility of a pseudogap opening at a characteristic temperature (T^*) well above the transition temperature (T_C), which is indicative of partial-pair formation induced by some excitation in the electronic states. The most important problem is how partial-normal-state pairing and Cooper pairing are related to each other.

However, such unusual behaviors have not been reported for high-frequency properties of charged carriers in the terahertz (THz) frequency region. One reason is that almost all of the experiments using THz probes have not used underdoped samples. They have concentrated instead on well-characterized HTSC thin films, particularly on $\text{YBa}_2\text{Cu}_3\text{O}_{7-\delta}$ (YBCO) thin films optimally doped. [7, 8] However, if the interaction energy characterizing the normal-state partial correlation is of the order of several meV (\sim THz), some resonance effects should be detectable with use of a THz probe.

Recently, Corson *et al.* pointed out that high-frequency probes may be able to detect partial phase coherence in the normal state of an underdoped HTSC if the correlation times are sufficiently short. They carried out time-domain terahertz transmission spec-

troscopy (TDTTS) on thin epitaxial films of underdoped $\text{Bi}_2\text{Sr}_2\text{CaCu}_2\text{O}_{8+\delta}$ (BSCCO). [9] At high frequencies from 0.1 to 0.6 THz, they observed broad transition from the normal to the superconducting state of σ_2 below 100 K, but observed no obvious sign of T^* well above T_C even in the most underdoped sample with a T_C of 33 K.

We investigated the higher-frequency properties of BSCCO thin film by TDTTS at frequencies from 0.3 to 1.5 THz. In this letter we report experimental observations of the high-frequency properties that showed strong evidence of partial-pair formation below $T^* \simeq 210 \text{ K}$ around a characteristic frequency of $f_{C1} \simeq 1.3 \text{ THz}$. Conversely, the long-range phase coherence responsible for superconductivity below T_C was primarily distinguished by lower frequency carriers ($f < f_{C2} \simeq 0.5 \text{ THz}$).

For our experiments, we used an as-grown thin film, about 50-nm thick grown by laser ablation on a MgO (100) substrate ($10 \times 10 \times 0.5 \text{ mm}$). [10] Thin-film characterization was carried out using X-ray diffraction (XRD), atomic force microscopy (AFM), and critical supercurrent density (J_C) measurements. The XRD patterns showed that all diffraction peaks were indexed by $(00l)$ of $\text{Bi}_2\text{Sr}_2\text{CaCu}_2\text{O}_{8+\delta}$ single phase and that the film was c-axis oriented. The AFM study showed that the surface was composed of a lot of small grains sub- μm in size with the averaged root-mean-square value of about 4 nm.

The sample showed superconducting transition at $T_{C01} = 76 \text{ K}$ and $T_{C02} = 58 \text{ K}$, corresponding to the

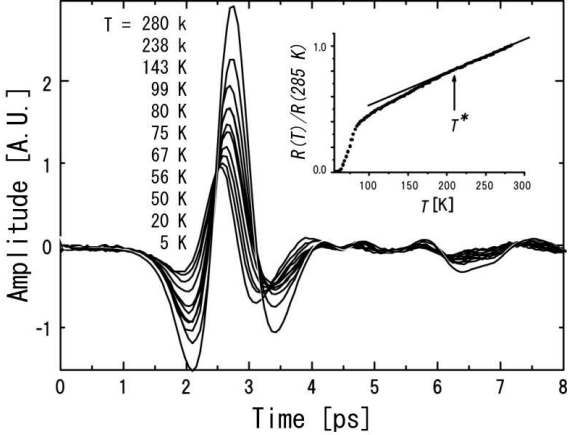


FIG. 1: Transmitted THz pulse signals observed at several temperatures. Here, only the first leading pulses are displayed for clarity. Phase shift took place below 75 K and settled below about 50 K due to high-pass filter property of superconducting thin film. The inset shows temperature dependence of in-plane resistance when a current density of $J = 4 \times 10^3 \text{ A/cm}^2$ was applied along the ab-plane.

current density of $J_{C1} = 33 \text{ A/cm}^2$, and $J_{C2} = 4 \times 10^3 \text{ A/cm}^2$, respectively. The current density gradually increased below T_{C01} and rapidly increased below T_{C02} with decreasing temperature. The observed maximum value of $J_{Cmax} = 4.3 \times 10^5 \text{ A/cm}^2$ at $T = 10 \text{ K}$ was about one order of magnitude lower than that of optimally doped BSCCO film described in Ref. 11. These observed behaviors in J_C show that majority part of the thin film was composed of low T_C phase with the critical temperature T_{C02} and the low J_C value.

For the TDTTS measurements, we used femtosecond optical pulses with a pulse width of about 100 fs (full-width at half maximum) as optical sources. The optical pulses were generated by a mode-locked Ti:Sapphire laser with a center wavelength of 810 nm and a repetition rate of 82 MHz. For wide-range measurements, dipole-antenna-type photoconductive switches formed on low-temperature-grown GaAs films were used as the THz electromagnetic-wave emitter and detector. The sample was mounted on a 6-mm ϕ -hole in a copper finger of an open-cycled liquid-He cryostat placed between a pair of paraboloidal mirrors, and the sample room was vacuumed to about 10^{-6} Torr. We observed the transmittance of a MgO substrate as a reference by using a same-sized MgO substrate in place of the sample. Using this experimental setup, we could measure the temperature dependence of THz transmittance at temperatures between 4.2 K and room temperature.

The Fourier components of the transmitted electric fields, $E_{sample}(\omega, \phi)$ and $E_{ref}(\omega, \phi)$, were obtained through fast Fourier transformation. From the Fourier components, we extracted the complex transmittance, $t(\omega, \phi)$, of the thin film itself by dividing $E_{sample}(\omega, \phi)$ by $E_{ref}(\omega, \phi)$. For accuracy, we directly determined

the complex refractive index numerically by minimizing the difference between the experimental $t(\omega, \phi)$ and theoretical one given by Born *et al.* [12] without using Kramers-Kronig analysis. Then, the complex conductivity, $\sigma = \sigma_1 + i\sigma_2$, and the surface impedance, $Z_S = R_S + iX_S$, of the thin film were directly calculated. The details of our optical system and data processing have been reported elsewhere. [13]

Figure 1 shows transmitted THz pulse signals for several temperatures. For clarity, only the first leading pulses are displayed. The inset shows the temperature dependence of normalized resistance with a current density of $J = 4 \times 10^3 \text{ A/cm}^2$ applied along the ab-plane. The amplitude of the leading pulses decreased coincident with the resistive transition, and settled at an almost constant value below $T \simeq T_{C02}$. This demonstrated that long-range phase coherence occurred all over the sample immediately under T_{C02} . That characteristic is also seen in Fig. 1, where THz pulses below T_{C02} have a time-differential shape compared to those in the normal state. This change in the pulse shape from the normal to the superconducting state has been well explained using a shunt inductor model for the transmission line acting as a high-pass filter in the superconducting state. [14]

The temperature dependences of the real and imaginary parts of complex conductivity, σ_1 and σ_2 , for several frequencies are displayed in Figs. 2(a) and 2(b), respectively. The maximum values of σ_1 and σ_2 observed for 0.33 THz were about one order of magnitude lower than those for 0.1 THz reported in Ref. 9. The difference is mainly due to the probing frequency and the film quality because these values show strong frequency dependence in $f < 0.5 \text{ THz}$, and the sample described in Ref. 9 was prepared by atomic layer-by-layer molecular-beam epitaxy. [15]

In Fig. 2(a) σ_1 displays the broad coherence-like peaks centered near T_{C02} for frequencies below 1.0 THz, and near 80 K for 1.25 and 1.5 THz. The lower frequency properties for $f \leq f_{C2}$ further show a local maximum at temperatures below 20 K, which is interpreted as related to the increase in scattering time of quasi-particles below T_C . [16]

Conversely, σ_2 (Fig. 2(b)) shows a noteworthy phenomenon in the high-frequency region. The higher-frequency σ_2 ($0.8 \text{ THz} < f$) increases below a characteristic temperature of $T^* \simeq 210 \text{ K}$. This is clearly observable for 1.0, 1.25 and 1.5 THz in Fig. 2(b). On the other hand, the lower-frequency σ_2 ($f < f_{C2}$) is almost 0 above $\sim 100 \text{ K}$ and rapidly increases below T_{C01} showing fairly good consistency with the result observed in underdoped BSCCO film in Ref. 9. These anomalies observed in σ_2 show the property peculiar to underdoped sample, although it is hard to consider that deoxidization process naturally takes place in present as-grown thin film without any special treatments. However, considering the film thickness, the surface roughness, and the small grain size, deoxidization may takes place, particularly at the grain boundaries in vacuum condition.

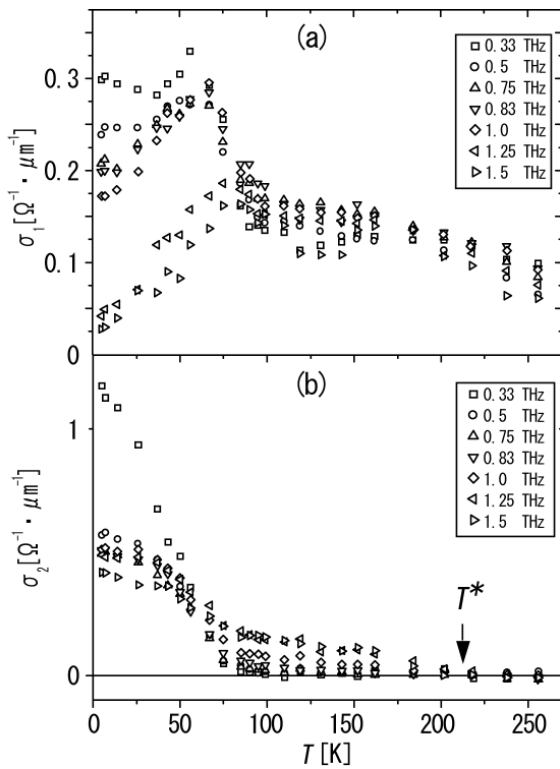


FIG. 2: Temperature dependence of (a) real and (b) imaginary parts of complex conductivity, $\sigma = \sigma_1 + i\sigma_2$, for several frequencies. The σ_2 showed a measurable increase below a characteristic temperature of $T^* \simeq 220$ K in the normal state for $f = 1.0, 1.25$ and 1.5 THz, and a rapid increase below T_{C01} particularly for $f = 0.33$ THz.

The experimental observation indicating a marked property of underdoped sample was also observed in the in-plane resistance. The inset of Fig. 1 shows the temperature dependence of the in-plane resistance, R . We can see that R deviates from the T -linear dependence below $\sim T^*$. Such deviation in the in-plane resistivity have been observed only on underdoped HTSC samples and explained as being related to spin excitation (or spin gap). [17] Current TDTTS research has no means to directly probe the spin excitation state, however, a little effect on the electronic state may be detected.

Normal state anomalies in the higher frequency regions were also observed within other parameters. Corresponding to the results above, surface reactance, $X_S(T)$, also showed anomalous behavior. Figure 3 shows the temperature dependence of X_S for several frequencies. Normalized values, $X_S(T)/X_S(110K)$, are plotted for clarity, and the X_S value at $T = 110$ K is also displayed for each frequency. We can see an obvious decrease around T^* with decreasing temperature in the transition curves for 1.25 and 1.4 THz. The transitions take place step-by-step near T^* and T_{C01} , respectively, and settle at lower values at $T = 5$ K than those for lower frequencies.

The temperature dependence of surface resistance R_S showed a slight resistive drop near T^* and a rapid de-

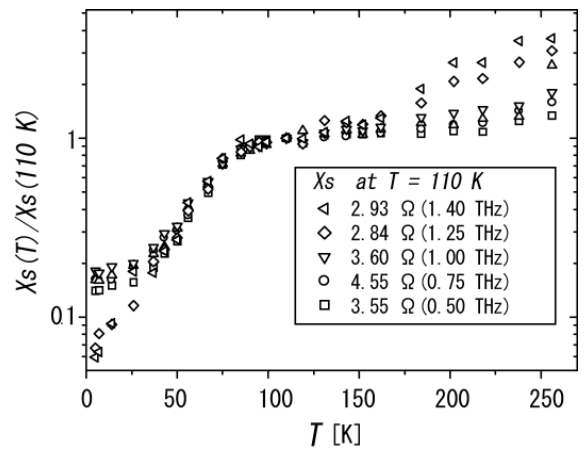


FIG. 3: Temperature dependence of normalized surface reactance, $X_S(T)/X_S(110K)$, obtained for several frequencies. Inset shows X_S value obtained at $T = 110$ K for each frequency.

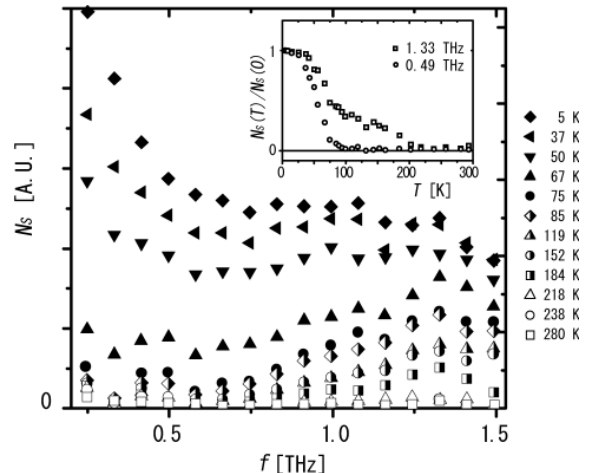


FIG. 4: Frequency dependence of density of supercarrier, N_S , for several temperatures. Inset shows temperature dependence of normalized density of supercarriers, $N_S(T)/N_S(0)$, near characteristic frequencies, 0.49 and 1.33 THz.

crease near T_{C01} at frequencies above 1.0 THz. It also showed an interesting frequency dependence, approximately according with the power laws of $R_S \propto f$ ($f < 0.5$ THz and 1.0 THz $< f$) and $R_S \propto f^{0.5}$ (0.5 THz $< f < 1.0$ THz) in the superconducting state, and $R_S \propto f$ (1.0 THz $< f$) and $R_S \propto f^{0.5}$ ($f < 1.0$ THz) in the normal state. The details of the observed characteristics including the other optical parameters will be presented elsewhere.

As shown above, we gained experimental knowledge indicating the possibility of partial-pair formation below T^* accompanied by short-range phase coherence with characteristic correlation times of about one ps or less. Our greatest concern is how the long-range coherence (Cooper pairing below T_C) and the short-range coherence (partial

pairing below T^*) are related to each other. To investigate the problem, we simply estimated the density of supercarriers, N_S , by using the relationship,

$$N_S \propto \lambda_L^{-2} = \mu_0 \omega \sigma_2. \quad (1)$$

Figure 4 shows the frequency dependence of N_S . We ignored the Drude contribution from the normal carriers to σ_2 for simplicity. Therefore, the plotted data marked as half blank ($T_{C01} < T < T^*$), particularly as blank patterns ($T^* < T$), only provide rough estimates.

Limiting the discussion to the lower temperature regions below T_{C01} where the Drude contribution is almost negligible, we can see broad local maximums at frequencies around $f_{C1} \simeq 1.3$ THz (particularly above 67 K) and a rapid increase below f_{C2} (particularly below 50 K) in Fig. 4. As the temperature was increased from 5 K to T_{C01} , N_S strongly decreased at frequencies below f_{C2} , while about 50 % of the supercarriers still remained even at 75 K around f_{C1} . This means that partial-pairs are certainly formed even above T_{C01} as the result of the limited-correlation with the ultrafast carriers around f_{C1} . The limited partial-pairs, therefore, may have a weak effect on the transport property, as shown in the inset of Fig. 1. On the other hand, the increase in N_S was seen over all the frequencies below T_{C01} , although the increase below f_{C2} occurred more drastically than that in the higher frequency range. This shows that the long-range phase coherence responsible for the superconductivity (or Cooper pairing) was caused by correlation with wide-range carriers, particularly with ones below f_{C2} .

These relationships are more clearly shown in the in-

set of Fig. 4, if we ignore the Drude contribution. The inset shows that the normalized N_S values for $f = 0.49$ THz are almost 0 above ~ 100 K, showing no effect from the partial-pair formation. The plots for 1.33 THz show an increase in partial-pair density below T^* and an additional increase of Cooper pairing below T_{C01} . These results show the possibility that the short and long-range phase coherences are due to different pairing mechanisms.

In summary, TDTTS measurements were carried out on as-grown BSCCO thin film to investigate the high-frequency properties of carriers in the THz-frequency regions. The observed high-frequency properties and the temperature dependence of in-plane resistance showed a marked property of HTSC sample in underdoped regime. The frequency-resolved properties show strong evidence that partial-pair formation accompanied by short-range phase coherence certainly occurs below $T^* \simeq 210$ K with an ultrafast correlation time of one ps or less, due to the direct electronic excitation process or indirect excitation process induced by the spin excitation. Long-range phase coherence characterized by Cooper pairing formation below T_{C01} was found to be strongly related to lower frequency carriers below $f_{C2} \simeq 0.5$ THz. These experimental results show that the short and long-range phase coherences are based on different pairing mechanisms.

Acknowledgments

This work was supported in part by a Grant-in-Aid for Scientific Research (B), No. 12450146, from the Ministry of Education, Culture, Sports, Science and Technology.

- [1] H. Alloul *et al.*, Phys. Rev. Lett. **63**, 1700 (1989), and G. V. M. Williams *et al.*, Phys. Rev. Lett. **78**, 721 (1997).
- [2] J. Rossat-Mignod *et al.*, Physica C **185-189**, 86 (1991), and P. M. Gehring *et al.*, Phys. Rev. B **44**, 2811 (1991).
- [3] A. V. Puchkov *et al.*, Phys. Rev. Lett. **77**, 3212 (1996).
- [4] S. Uchida *et al.*, Physica C **263**, 264 (1996).
- [5] Ch. Renner *et al.*, Phys. Rev. Lett. **80**, 149 (1997).
- [6] H. Ding *et al.*, Nature (London) **382**, 51 (1996), and A. G. Loeser *et al.*, Science **273**, 325 (1996).
- [7] I. Wilke *et al.*, J. Appl. Phys. **87**, 2984 (2000).
- [8] T. Kiwa *et al.*, Physica C, in press.
- [9] J. Corson *et al.*, Nature **398**, 221 (1999).
- [10] T. Uchiyama *et al.*, IEEE Appl. Super., in press.
- [11] J. Otsuka *et al.*, Physica C **331**, 164 (1999).
- [12] M. Born *et al.*, *Principles of Optics*, 5th ed. (Pergamon, New York, 1975).
- [13] T. Kiwa *et al.*, Jpn. J. Appl. Phys. **40**, L 38 (2001).
- [14] S. D. Brorson *et al.*, Phys. Rev. B **49**, 6185 (1993).
- [15] J. N. Eckstein *et al.*, Annu. Rev. Mater. Sci. **25**, 679 (1995).
- [16] J. Corson *et al.*, Phys. Rev. Lett. **85**, 2569 (2000).
- [17] T. Ito *et al.*, Phys. Rev. Lett. **70**, 3995 (1993).